Superconductivity in one-atomic-layer metal films grown on Si(111)

Tong Zhang[1,2], Peng Cheng[1], Wen-Juan Li[1,2], Yu-Jie Sun[1], Guang Wang[1], Xie-Gang Zhu[1], Ke He[2], Lili Wang[2], Xucun Ma[2], Xi Chen[1]*, Yayu Wang[1], Ying Liu[3], Hai-Qing Lin[4], Jin-Feng Jia[1] and Qi-Kun Xue[1,2]*

The two-dimensional (2D) superconducting state is a fragile state of matter susceptible to quantum phase fluctuations. Although superconductivity has been observed in ultrathin metal films down to a few layers[1-10], it is still not known whether a single layer of ordered metal atoms, which represents the ultimate 2D limit of a crystalline film, could be superconducting. Here we report scanning tunnelling microscopy measurements on single atomic layers of Pb and In grown epitaxially on Si(111) substrate, and demonstrate unambiguously that superconductivity does exist at such a 2D extreme. The film shows a superconducting transition temperature of 1.83 K for an atom areal density $n = 10.44$ Pb atoms nm^{-2}, 1.52 K for $n = 9.40$ Pb atoms nm^{-2} and 3.18 K for $n = 9.40$ In atoms nm^{-2}, respectively. We confirm the occurrence of superconductivity by the presence of superconducting vortices under magnetic field. *In situ* angle-resolved photoemission spectroscopy measurements reveal that the observed superconductivity is due to the interplay between the Pb–Pb (In–In) metallic and the Pb–Si (In–Si) covalent bondings.

The one-atomic-layer films of Pb and In studied here were grown with atomic precision on bulk-terminated Si(111) substrate using molecular beam epitaxy. The one-atomic-layer films of Pb have two different structural phases depending on the coverage (for sample preparation, see the Methods section). Figure 1a,d shows the schematic structure and scanning tunnelling microscopy (STM) topograph of the so-called striped incommensurate (SIC) phase, which has a Pb coverage of 4/3 monolayers (ML; refs 11–14). Here 1 ML is defined as the surface atomic density of the Si(111) with areal density $n = 7.84$ atoms nm^{-2}. In a unit cell of the SIC-Pb phase, there are four Pb atoms per three surface Si atoms. Three of the four Pb atoms each form a covalent bond with an underlying Si atom, leaving one Pb atom without bonding to the Si substrate. Besides the covalent bonds with the Si substrate, the metal atoms also form metallic bonds within the metal overlayer. As all Pb atoms are located exactly in the same atomic-layer sheet (see the large-scale STM image and cross-section height profiles in Supplementary Fig. S1), the resulting areal density of Pb atoms is 10.44 nm^{-2}. Compared with the bulk Pb(111) plane, the lattice of the SIC phase is compressed by 5%.

Ultralow-temperature (down to 0.40 K) scanning tunnelling spectroscopy (STS) on the SIC phase reveals a clear signature of superconductivity. Figure 2a shows the tunnelling spectra taken on the SIC phase using a superconducting Nb tip. At 0.42 K, the differential conductance shows a zero conductance region near the Fermi level (E_F) and two sharp peaks at bias voltages $V \sim \pm 1.8$ meV. This is the classical hallmark of a superconductor–insulator–superconductor (SIS) tunnelling junction, which has a zero quasiparticle density of states (DOS) at E_F and two Bardeen–Cooper–Schrieffer (BCS)-like DOS peaks at $V = \pm(\Delta_{tip} + \Delta_{SIC})/e$. Here Δ_{tip} and Δ_{SIC} are the superconducting gaps of the Nb tip and the SIC phase, respectively; e is the electron charge. Starting from 1.05 K, two extra peaks at $V = \pm(\Delta_{tip} - \Delta_{SIC})/e$ become evident. This is caused by thermally excited holes/electrons[15]. The observation also demonstrates the high energy resolution of our STS measurements[16,17]. With increasing temperature, the spectra are broadened and the coherence peaks are suppressed. The energy gap Δ_{SIC} becomes nearly invisible at 1.82 K, suggesting that the superconducting transition occurs around this temperature. The superconducting characteristics are further demonstrated by using a non-superconducting PtIr tip (Supplementary Fig. S2). Using a superconducting gap $\Delta_{tip} = 1.46$ meV ($T_C = 9$ K) for the Nb tip, which was calibrated by a separate measurement on Ag islands (Supplementary Fig. S3), we obtain the temperature evolution of Δ_{SIC}, as shown in Fig. 2b. Fitting the data using the BCS gap function[18] yields $\Delta_{SIC}(0) = 0.35$ meV, $T_C = 1.83$ K and the BCS ratio $2\Delta_{SIC}/k_B T_C = 4.4$ (k_B is the Boltzmann constant). The BCS ratio is very close to the value of 4.3 in bulk Pb, suggesting that the SIC phase is a strongly coupled BCS superconductor.

Another one-atomic-layer film of Pb has the same fundamental $\sqrt{7} \times \sqrt{3}$ building block as SIC but a smaller coverage of 6/5 ML (refs 12–14, 19–21). Hereafter this is called the $\sqrt{7} \times \sqrt{3}$-Pb phase (Fig. 1b,e). In a unit cell of the $\sqrt{7} \times \sqrt{3}$-Pb phase, there are six Pb atoms per five surface Si atoms. Five of the six Pb atoms each form a covalent bond with an underlying Si atom, leaving one Pb atom without bonding to the Si substrate. The areal atom density is nearly the same as that of the bulk Pb(111) plane, with a slight lattice expansion of 0.1%. Figure 2c shows the tunnelling spectra of the SIS junction in the $\sqrt{7} \times \sqrt{3}$-Pb phase, which is qualitatively the same as that of the SIC phase, except for a reduction of the energy gap. The superconducting gap Δ, T_C and the $2\Delta/k_B T_C$ ratio deduced from the BCS fitting of the experiment are 0.27 meV, 1.52 K and 4.12, respectively (Fig. 2d).

Indium atoms grow on Si(111) with the same $\sqrt{7} \times \sqrt{3}$ structure as that of Pb (refs 22, 23) (Fig. 1c,f). The In coverage is 6/5 ML, and the areal atom density is 9.40 nm^{-2}. Thus, its lattice is 0.3% expanded compared with that of the bulk In(001) plane. Figure 2e
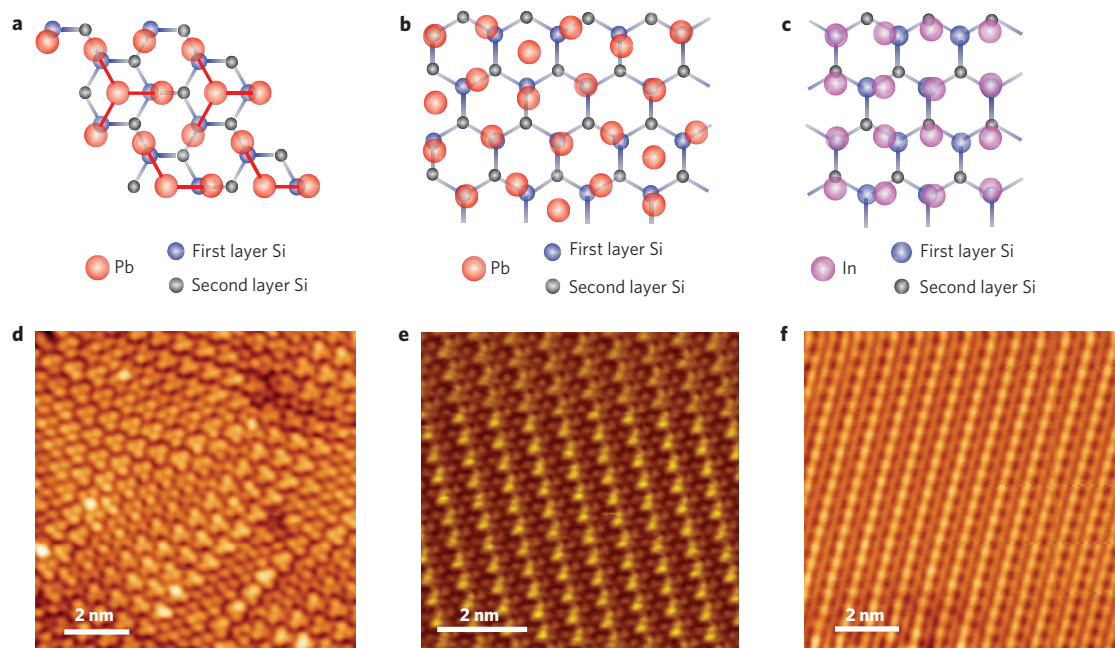
Figure 1 | One-atomic-layer superconducting metal films of Pb and In. a–f, Schematic structure models[11–14,19,22] (**a–c**) and high-resolution STM images (**d–f**) of the SIC-Pb (**a,d**), $\sqrt{7}\times\sqrt{3}$-Pb (**b,e**) and $\sqrt{7}\times\sqrt{3}$-In (**c,f**) phases grown on Si(111) substrate. Imaging conditions are $V = 0.1$ V and $I = 0.05$ nA.
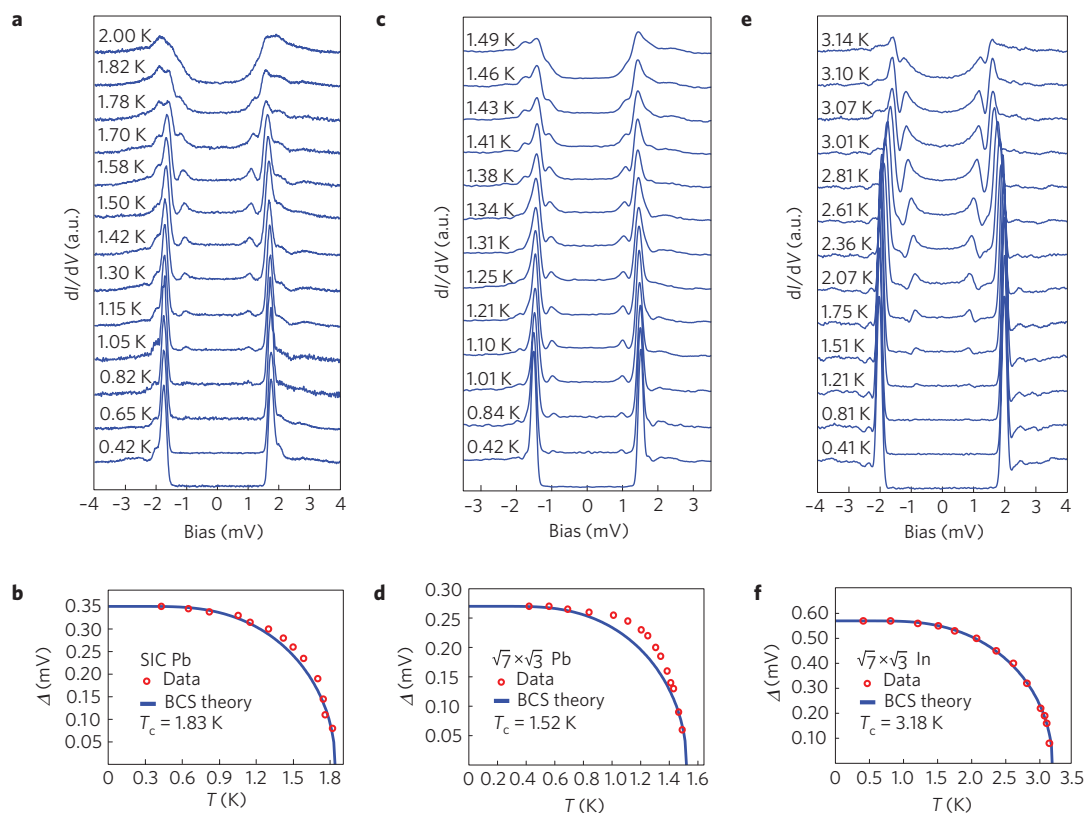

Figure 2 | Superconductivity in one-atomic-layer metal films. a, The differential conductance of single-particle tunnelling measured with a Nb tip on the SIC-Pb phase as a function of temperature. The tunnelling junction (also applies to **c** and **e**) was set at $V = 0.01$ mV and $I = 0.2$ nA. The curves at different temperatures are offset vertically for clarity. **b**, The superconducting gap of the SIC-Pb phase as a function of temperature. The open circles show the measured gap, and the solid curve shows the fitting by the BCS gap function (see the text). **c–f**, The tunnelling conductance (**c,e**) and superconducting gap (**d,f**) for the $\sqrt{7}\times\sqrt{3}$-Pb (**c,d**) and $\sqrt{7}\times\sqrt{3}$-In (**e,f**) phases.

shows the tunnelling spectra of the $\sqrt{7}\times\sqrt{3}$-In phase. The values of Δ, T_C and $2\Delta/k_B T_C$ extracted from the BCS fit (Supplementary Fig. S4) are 0.57 meV, 3.18 K and 4.16, respectively (Fig. 2f). Unlike

the Pb films, where T_C is strongly suppressed compared with the bulk value, the $\sqrt{7}\times\sqrt{3}$-In phase has a surprisingly high T_C close to the bulk value 3.4 K, as predicted previously[23]. More significantly,
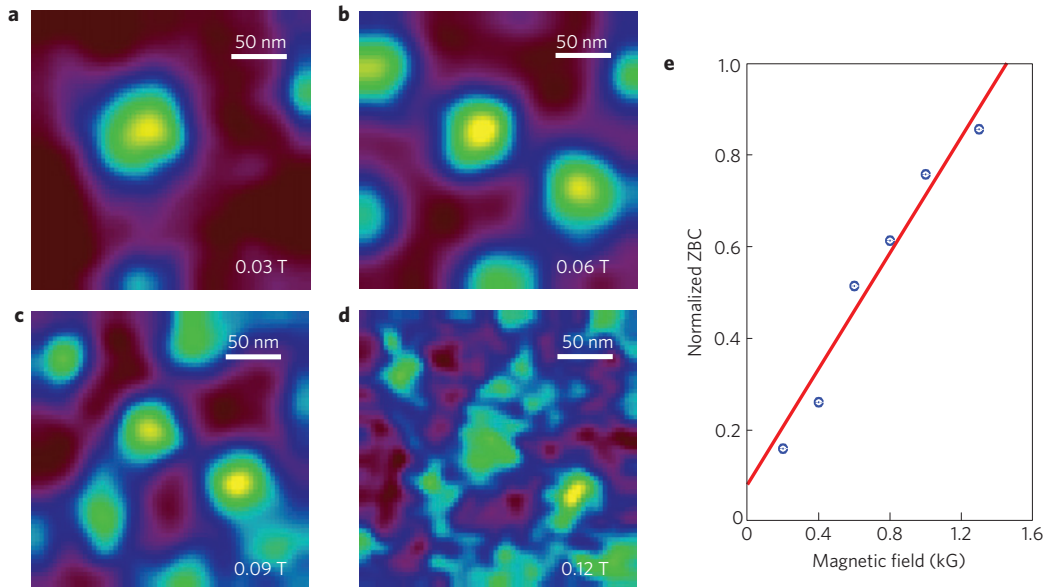
Figure 3 | Superconducting vortices in the SIC-Pb phase. a–d, The vortices at different magnetic fields (0.03–0.12 T) measured at 0.42 K using a PtIr tip. In each vortex image, the superconducting regions of low conductance are shown in maroon colour and the gapless normal state inside the vortex cores are yellow coloured. The tunnelling junction was set at $V = 0.01$ mV and $I = 0.1$ nA. The bias voltage was ramped to 0 V with feedback off at each pixel to record the ZBC. **e**, Normalized ZBC measured at locations between two vortices under different magnetic fields. The upper critical field of the SIC phase is estimated to be 1450 G.

the enhanced $2\Delta/k_B T_C$ ratio compared with the bulk (3.6) implies that it is transformed into a strongly coupled superconductor by reducing the dimension.

The occurrence of superconductivity in the one-atomic-layer films is further confirmed by the presence of superconducting vortices under magnetic field. The magnetic measurement on the SIC phase is shown in Fig. 3 and Supplementary Fig. S5. As seen in the zero bias conductance (ZBC) spectra mapping, the vortices start to form at a field of around 0.03 T (Fig. 3a), and increase in density with the field (Fig. 3b,c). The vortex image becomes severely blurred at $B \sim 0.12$ T (Fig. 3d), suggesting that the superconducting state is almost completely suppressed around this field. From a systematic field-dependence study of ZBC (ref. 24), an upper critical field H_{C2} of 1,450 G is obtained (Fig. 3e). In a type II superconductor, $H_{C2}(T)$ is determined by the coherence length ξ_{GL} through $H_{C2}(T) = \Phi_0/2\pi\xi_{GL}^2(T)$, where Φ_0 is the magnetic flux quanta. The 1,450 G upper critical field renders a coherence length $\xi_{GL} = 49$ nm, which tells us the size of the Cooper pair and vortex core in this phase.

To understand the mechanism of the superconductivity in these one-atomic-layer superconductors, we have carried out high-resolution angle-resolved photoemission spectroscopy (ARPES) measurements[3,25]. The electronic structure revealed by ARPES shows that despite the extreme 2D geometry and the coupling with the Si substrate, the one-atomic-layer films show well-developed 2D free-electron-like metallic bands[21,23]. Figure 4a shows an ARPES spectrum of the SIC phase along the $\bar{\Gamma}$–$\bar{M}$($\bar{\Gamma}$–$\bar{K}'$–$\bar{M}'$) direction at $T = 30$ K. $\bar{\Gamma}$, $\bar{M}$, $\bar{K}$ and $\bar{\Gamma}'$, $\bar{M}'$, $\bar{K}'$ denote the symmetry points of 1×1 and $\sqrt{3} \times \sqrt{3}$ surface Brillouin zones (SBZs) of Si(111), respectively. Two parabolic bands (red solid lines in Fig. 4a) crossing E_F are centred at 0.62 and 1.26 Å^{-1} (the $\bar{K}'$ points), which are attributed to the surface states of SIC because they are situated above the edge of Si bulk bands[21]. The ARPES data along the $\bar{\Gamma}$–$\bar{K}$($\bar{\Gamma}$–$\bar{M}'$–$\bar{\Gamma}'$) direction (not shown) reveal other parabolic surface bands with larger Fermi circles centred on $\bar{\Gamma}$ and $\bar{K}(\bar{\Gamma}')$. Therefore, the surface states of SIC reflect the $\sqrt{3} \times \sqrt{3}$ periodicity with a large electron pocket at $\bar{\Gamma}'$ and a small one at $\bar{K}'$ (Fig. 4b). The total sheet carrier density estimated by the sizes of the two kinds of electron pocket is

about 9×10^{14} cm^{-2}. The ARPES data for $\sqrt{7} \times \sqrt{3}$-Pb are shown in Fig. 4c,d, and agree with the previous study[21]. Despite a different Fermi-surface shape, its electronic structure (as well as that of the $\sqrt{7} \times \sqrt{3}$-In; ref. 23) could also be understood on the basis of a 2D free-electron-like band.

The Si substrates used for the growth of the one-atomic-layer films shown above are heavily doped with boron (hole concentration $\sim 8 \times 10^{18}$ cm^{-3}). To clarify the possible role of the dopants on superconductivity, we have studied the SIC-Pb phases prepared on both heavily p-type (4×10^{19} cm^{-3}) and normally n-type ($\sim 10^{16}$ cm^{-3}) doped Si substrates. The SIS spectra of the two films are shown together in Supplementary Fig. S6. The nearly identical results exclude any significant role of the dopants in Si, and suggest that the electronic property of the metal overlayer is dominated only by the intra-overlay metallic and the Pb–Si interface covalent bondings. In this sense, the superconducting films seem to be electronically 'isolated' from the underlying Si lattice. Thus, only the metal overlayer and the metal–Si interface are responsible for the occurrence of superconductivity.

We now discuss the possible roles of the Si substrate. Through the formation of covalent bonds at the interface[11–14,19–23], the Si substrate serves as a structural support stabilizing the crystal structure of the metal overlay. This is important because free-standing monolayer films of metals such as Pb or In are unstable, unlike graphene. To investigate whether Si takes part in the electron pairing, we have carried out a variable-temperature ARPES measurement where the dimensionless electron–phonon coupling parameter λ can be evaluated by the temperature-dependent photoemission spectra[26]. The result for the SIC phase is $\lambda = 1.07 \pm 0.13$ (for details, see Supplementary Fig. S7), which is greatly enhanced compared with the $\lambda < 0.9$ of the much thicker Pb films[25,27], apparently owing to the presence of the metal–Si interface. The strongly enhanced λ (~ 1) in the $\sqrt{7} \times \sqrt{3}$-In film[23] is particularly significant, because now its surprisingly high $T_C \sim 3.18$ K can be explained by the strong-coupling McMillan formula[28]. The similar λ values in the Pb and In films suggest that the phonon modes from interface bonding must contribute to electron–phonon coupling in a significant way[27].
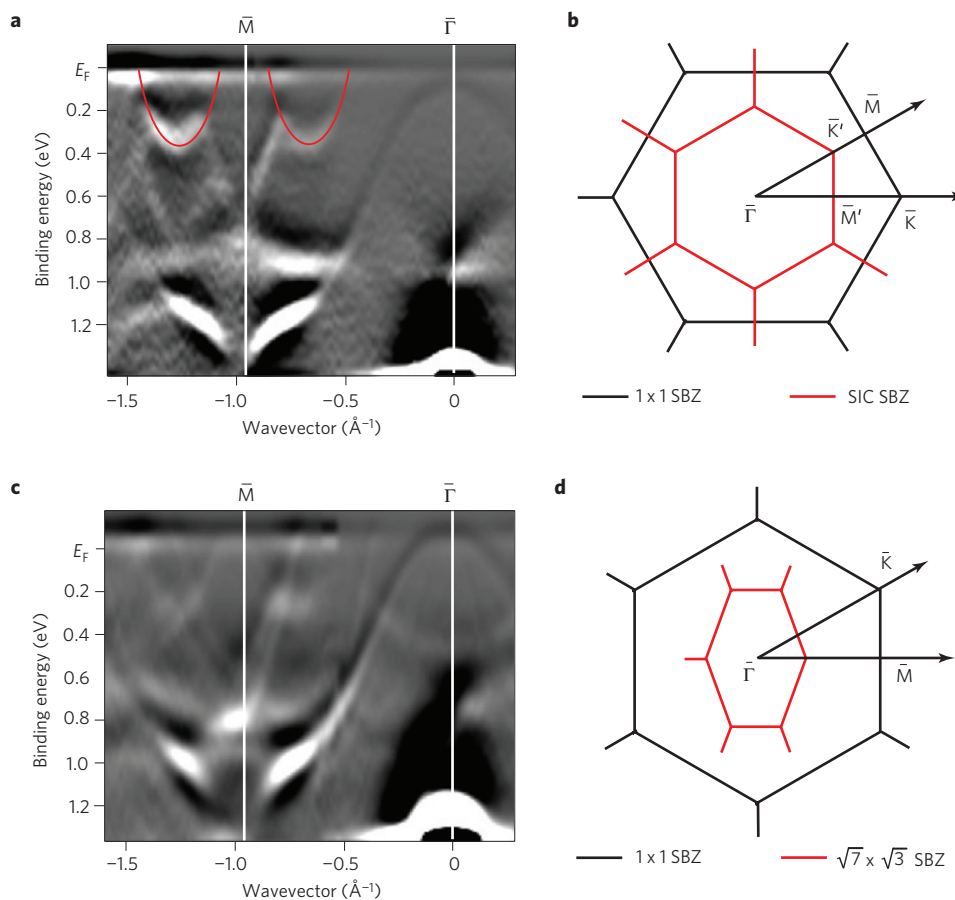
Figure 4 | The ARPES spectra of one-atomic-layer Pb films on Si. a, The energy band measured along the $\bar{\Gamma} - \bar{M}$ direction for the SIC phase on p-type Si at 30 K. The photon energy was 21.218 eV (He Iα). Free-electron-like bands (indicated by parabola) are observed around $k_\parallel = 0.6$ and 1.26 Å^{-1}. The parabolic feature centred at the $\bar{\Gamma}$ point near E_F and dispersing to higher binding energy is the edge of the Si bulk valence band. **b**, The SBZ of the SIC-Pb phase. **c**, The energy band measured along the $\bar{\Gamma}$-$\bar{M}$ direction for the $\sqrt{7} \times \sqrt{3}$-Pb phase on p-type Si at 30 K. **d**, The SBZ of the $\sqrt{7} \times \sqrt{3}$-Pb phase.

As for the intra-overlay metallic bonding, the development of nearly free-electron-like metallic bands seen in Fig. 4 implies that the supercurrent should be carried by the carriers in the metal overlay. The difference between SIC and $\sqrt{7} \times \sqrt{3}$-Pb further highlights the crucial role of the overlayer structure. The denser packing in the SIC phase leads to a stronger superconductivity, which remains an interesting subject to be further investigated.

These observations suggest a new route towards 2D superconductivity: the metal overlay serves as a charge reservoir and the electron–phonon interactions that glue the electrons to form pairs are provided both by the intralayer metallic and more importantly the interface bonds. The situation is rather different from that of the 2 ML Pb film superconductivity reported recently[9], which is essentially a property of the film itself with the same mechanism of superconductivity as that of thicker films.

Methods

To investigate the electronic structure and superconductivity of the one-atomic-layer films, we have used two ultrahigh-vacuum systems, both equipped with molecular beam epitaxy for film growth. The first system features an *in situ* ultralow-temperature STM system (Unisoku and RHK) operated at a base temperature of 0.40 K and under a magnetic field up to 11 T (refs 16, 17). The energy resolution is better than 0.1 meV at 0.40 K when a Nb tip is used[16]. This proves critical because the superconducting gap of the samples is well below 1 meV. The second system features *in situ* low-temperature STM (Omicron) and high-energy-resolution (10 meV) ARPES with a Scienta R4000 analyser[3,25]. To prepare high-quality samples, we used pure Pb (99.9999%) and In (99.9999%), which were respectively evaporated from two Knudsen cells for molecular beam epitaxy (Omicron). The clean Si(111)-7 × 7 surface was used as substrate for preparing the one-atomic-layer films of Pb and In. The Si(111)-7 × 7 surface was

prepared by cycles of annealing and flashing up to 1,480 K of the as-supplied Si wafer in the ultrahigh-vacuum chamber. The deposition rate of Pb or In and thus the metal coverage and film thickness was carefully calibrated by the Pb (In)-induced $\sqrt{3} \times \sqrt{3}$ phase on the clean Si(111) surface, which is known to have a precise surface coverage of 1/3 ML. The Pb-SIC phase was prepared by depositing ~1.5 ML Pb atoms on Si(111)-7 × 7 surface at room temperature and subsequently annealing at 550 K for 30 s. The deposition rate of Pb/In was 0.1 ML min^{-1}. The $\sqrt{7} \times \sqrt{3}$-Pb phase was prepared by annealing the SIC phase at 550 K for two minutes to reduce the Pb coverage. The $\sqrt{7} \times \sqrt{3}$-In phase was prepared by depositing ~1.5 ML In atoms on Si(111)-7 × 7 surface at room temperature and subsequently annealing at 700 K for 4 min. To ensure that the same phase is studied in two separate systems, in each experimental run the structure of the film was first checked by the atomically resolved STM images (Fig. 1d–f), followed by STS measurement of the characteristic electronic states near E_F (Supplementary Fig. S1d,e).

References

1. Shal'nikov, A. I. Superconducting thin films. *Nature* **142,** 74 (1938).
2. Haviland, D. B., Liu, Y. & Goldman, A. M. Onset of superconductivity in the two-dimensional limit. *Phys. Rev. Lett.* **62,** 2180–2183 (1989).
3. Guo, Y. *et al.* Superconductivity modulated by quantum size effects. *Science* **306,** 1915–1917 (2004).
4. Özer, M. M., Thompson, J. R. & Weitering, H. H. Hard superconductivity of a soft metal in the quantum regime. *Nature Phys.* **2,** 173–176 (2006).
5. Eom, D., Qin, S., Chou, M.-Y. & Shih, C. K. Persistent superconductivity in ultrathin Pb films: a scanning tunnelling spectroscopy study. *Phys. Rev. Lett.* **96,** 027005 (2006).
6. Nishio, T., Ono, M., Eguchi, T., Sakata, H. & Hasegawa, Y. Superconductivity of nanometer-size Pb islands studied by low-temperature scanning tunnelling microscopy. *Appl. Phys. Lett.* **88,** 113115 (2006).

7. Shanenko, A. A., Croitoru, M. D. & Peeters, F. M. Oscillations of the superconducting temperature induced by quantum well states in thin metallic films: Numerical solution of the Bogoliubov–de Gennes equations. *Phys. Rev. B* **75,** 014519 (2007).
8. Nishio, T. *et al.* Superconducting Pb island nanostructures studied by scanning tunnelling microscopy and spectroscopy. *Phys. Rev. Lett.* **101,** 167001 (2008).
9. Qin, S. Y., Kim, J. D., Niu, Q. & Shih, C. K. Superconductivity at the two-dimensional limit. *Science* **324,** 1314–1317 (2009).
10. Brun, C. *et al.* Reduction of the superconducting gap of ultrathin Pb islands grown on Si(111). *Phys. Rev. Lett.* **102,** 207002 (2009).
11. Seehofer, L., Falkenberg, G., Daboul, D. & Johnson, R. L. Structural study of the close-packed two-dimensional phases of Pb on Ge(111) and Si(111). *Phys. Rev. B* **51,** 13503–13515 (1995).
12. Horikoshi, K., Tong, X., Nagao, T. & Hasegawa, S. Structural phase transitions of Pb-adsorbed Si(111) surfaces at low temperatures. *Phys. Rev. B* **60,** 13287–13290 (1999).
13. Kumpf, C. *et al.* Structural study of the commensurate–incommensurate low-temperature phase transition of Pb on Si(111). *Surf. Sci.* **448,** L213–L219 (2000).
14. Chan, T. L. *et al.* First-principles studies of structures and stabilities of Pb/Si(111). *Phys. Rev. B* **68,** 045410 (2003).
15. Giaever, I. Electron tunnelling between two superconductors. *Phys. Rev. Lett.* **5,** 464–466 (1960).
16. Ji, S. H. *et al.* High-resolution scanning tunnelling spectroscopy of magnetic impurity induced bound states in the superconducting gap of Pb thin films. *Phys. Rev. Lett.* **100,** 226801 (2008).
17. Chen, X. *et al.* Probing superexchange interaction in molecular magnets by spin-flip spectroscopy and microscopy. *Phys. Rev. Lett.* **101,** 197208 (2008).
18. Bardeen, J., Cooper, L. N. & Schrieffer, J. R. Theory of superconductivity. *Phys. Rev.* **108,** 1175–1204 (1957).
19. Brochard, S. *et al.* *Ab initio* calculations and scanning tunnelling microscopy experiments of the Si(111)-$\sqrt{7}\times\sqrt{3}$-Pb surface. *Phys. Rev. B* **66,** 205403 (2002).
20. Hupalo, M., Schmalian, J. & Tringides, M. C. Devil staircase in Pb/Si(111) ordered phases. *Phys. Rev. Lett.* **90,** 216106 (2003).
21. Choi, W. H., Koh, H., Rotenberg, E. & Yeom, H. W. Electronic structure of dense Pb overlayers on Si(111) investigated using angle-resolved photoemission. *Phys. Rev. B* **75,** 075329 (2007).
22. Kraft, J., Surnev, S. L. & Netzer, F. P. The structure of the indium-Si(111) ($\sqrt{7}\times\sqrt{3}$) monolayer surface. *Surf. Sci.* **340,** 36–48 (1995).
23. Rotenberg, E. *et al.* Indium $\sqrt{7}\times\sqrt{3}$ on Si(111): A nearly free electron metal in two dimensions. *Phys. Rev. Lett.* **91,** 246404 (2003).
24. Bergeal, N. *et al.* Scanning tunnelling spectroscopy on the novel superconductor CaC_6. *Phys. Rev. Lett.* **97,** 077003 (2006).
25. Zhang, Y. F. *et al.* Band structure and oscillatory electron–phonon coupling of Pb thin films determined by atomic-layer-resolved quantum-well states. *Phys. Rev. Lett.* **95,** 096802 (2005).
26. McDougall, B. A., Balasubramanian, T. & Jensen, E. Phonon contribution to quasiparticle lifetimes in Cu measured by angle-resolved photoemission. *Phys. Rev. B* **51,** 13891–13894 (1995).
27. Luh, D.-A., Miller, T., Paggel, J. J. & Chiang, T.-C. Large electron–phonon coupling at an interface. *Phys. Rev. Lett.* **88,** 256802 (2002).
28. McMillan, W. L. Transition temperature of strong-coupled superconductors. *Phys. Rev.* **167,** 331–344 (1968).

Acknowledgements

Author contributions

T.Z., P.C., W.-J.L., Y.-J.S., G.W. and X.-G.Z. carried out the experiments; K.H., L.W., X.M., Y.W., Y.L. and H.-Q.L. analysed the data; X.C., J.-F.J. and Q.-K.X. designed and coordinated the experiments; Q.-K.X. wrote the paper. All authors discussed the results and commented on the manuscript.

Additional information

The authors declare no competing financial interests. Supplementary information accompanies this paper on www.nature.com/naturephysics. Reprints and permissions information is available online at http://npg.nature.com/reprintsandpermissions. Correspondence and requests for materials should be addressed to X.C. or Q.-K.X.